A Model Study of Internal Tides in Coastal Frontal Zone*

DAKE CHEN, HSIEN WANG OU, AND CHANGMING DONG

Lamont-Doherty Earth Observatory of Columbia University, Palisades, New York

(Manuscript received 18 December 2001, in final form 12 July 2002)

ABSTRACT

Internal tides near a midlatitude shelf–slope front are studied using an idealized numerical model, with emphasis on their structure, energetics, and mixing effects. It is found that the properties of internal tides are highly dependent on frontal configuration and tidal frequency. At a winter front, energetic internal tides are generated and arrested in the frontal zone; the cross-shelf flow tends to be surface (bottom) intensified by a large internal circulation cell at the diurnal (semidiurnal) frequency. At a summer front, the diurnal internal tide is still trapped, but a semidiurnal internal tide propagates out of the frontal zone in the offshore direction while arrested at the inshore boundary. The presence of the shelf–slope front enhances the generation of internal tides, and it also causes an amplification of the semidiurnal internal tide by trapping its energy in the frontal zone. This amplification is most prominent at the offshore boundary of the winter front and the inshore boundary of the summer front, where strong tidal refraction takes place. Internal tides can cause significant mixing and dispersion in the frontal zone, with the semidiurnal internal tide being most effective toward the frontal boundaries, and the diurnal internal tide more effective near the site of generation.

1. Introduction

Internal tides and coastal fronts are both frequently discussed topics in oceanographic literature, but they have rarely been studied in the same context and little attention has been paid to the interaction between them. Traditional theories of internal tides are based on linear, inviscid models with only vertical stratification (e.g., Wunsch 1975; Baines 1982), and thus they are not readily applicable to coastal frontal regions where sharp horizontal density gradient and strong mixing exist. On the other hand, models of frontal dynamics usually do not explicitly take into account the effect of internal tides, although it has been suggested that internal tides could provide a significant energy source for mixing in coastal frontal zones (e.g., Huthnance 1989; Brickman and Loder 1993). In this study, we use a primitive-equation coastal ocean model to examine the generation, propagation, and dissipation of internal tides in the coastal frontal zone near the continental shelf break.

There is an increasing number of studies in which primitive-equation numerical models were applied to investigating tidal motions near the shelf break or bank edge. For example, Lamb (1994) used a nonhydrostatic model to simulate the formation of internal wave bores by strong cross-shelf tidal flow, though his model was inviscid and assumed a horizontally uniform stratification. Holloway (1996) studied the internal tides over a cross section of the Australian North West Shelf with a two-dimensional version of the Princeton Ocean Model, but he also initialized his model with level isopycnals. Chen and Beardsley (1995, 1998), using the same Princeton Ocean Model, examined the tidal rectification and mixing over Georges Bank. They were able to produce not only internal tides but also a tidal front at the bank edge, yet they did not try to explore the relation between the two. In their model, the net effect of internal tides was difficult to estimate because it could not be clearly separated from that of the surface tide.

The hydrography near the shelf break is often characterized by a seasonally varying density front. During wintertime, vertical stratification is largely destroyed by surface cooling and wind stirring, and the fresher shelf water is separated from the slope water by a front that intersects both the bottom and the sea surface, a common feature found along the mid-Atlantic seaboard of the North America. During summertime, a seasonal thermocline is formed in the upper water column by increased insolation and diminished wind, but it may not extend onto the shelf in regions of strong tidal currents and shallow water depth. In such a case the tidally mixed shelf water is separated from the stratified slope water by a double front: a lower branch that intersects the bottom and an upper branch that intersects the sea

* Lamont-Doherty Earth Observatory Contribution Number 6326.

Corresponding author address: Dr. Dake Chen, Lamont-Doherty Earth Observatory, Columbia University, Palisades, NY 10964.
E-mail: dchen@ldeo.columbia.edu

surface, both of which merge to the seasonal thermocline offshore. The internal tides at a summer front may differ significantly from those at a winter front because internal tidal energy can radiate away from the former but not from the latter.

The theoretical work of Ou and Maas (1988) is of particular relevance to the present study. They examined the internal tides at a winter shelf–slope front using a two-layer analytical model in which the interface intersects both the bottom and the surface. According to their model solution, internal tides should cause a surface (bottom) intensification of the cross-shelf flow at the diurnal (semidiurnal) frequency, and the semidiurnal tide should be preferentially amplified due to the presence of superinertial eigenmodes. Another study of relevance here is the earlier work of Chuang and Wang (1981). They developed a finite difference model of the linear wave equations to evaluate the effects of a fixed density front on internal tides. Their front merges to level isopycnals away from the frontal zone, thus in a way resembling the summer condition. They found that a shelf–slope front has strong effects on the generation and propagation of internal tides, and that these effects are highly sensitive to the orientation of the front.

Here we evaluate the effects of both winter and summer fronts on internal tides, as well as the roles of internal tides in these two different frontal regimes. In particular, we address the following questions: What is the structure of internal tides in the presence of a front? How does this structure vary from winter to summer fronts and from diurnal to semidiurnal tides? What controls the distribution and partition of internal tidal energy in the frontal zone? And how do internal tides contribute to the mixing and dispersion of passive tracers? The rest of this paper is organized as follows. The model configuration is described next in section 2. The general results for winter and summer fronts are presented in sections 3 and 4, respectively. The energetics of internal tides is considered in section 5 and the mixing effects of them in section 6. Last, a summary and some discussion are given in section 7.

2. Model configuration

The model used in this study is the primitive equation, free-surface, coastal ocean model originally developed by Wang (1982, 1985). It has been applied to various coastal studies, including simulations of the upwelling front off the northern California coast (Chen and Wang 1990) and the tidal front in the Celtic Sea (Wang et al. 1990). In the present version of the model, we use the Mellor and Yamada (1982) level 2.5 turbulence closure for vertical mixing, Smagorinsky's (1963) parameterization for horizontal mixing, and the Smolarkiewicz (1984) antidiffusive scheme for density and tracer advection. These features are essential for minimizing nonphysical mixing and maintaining a sharp front in the model. Another modification is that here we directly solve for density field instead of temperature and salinity so that the equation of state is not needed. Although this model by design is fully three-dimensional, it is configured in this study on a two-dimensional cross-shelf section and uniformity is assumed in the alongshelf direction. The effectiveness of this simplification has been demonstrated by numerous previous studies, including those cited in the last section.

The model is placed at 41°N so that the local inertial period is about 17 h. Since the model location is north of the critical latitude for the diurnal tide but south of that for the semidiurnal tide, the diurnal internal tide is expected to be trapped in the region of generation while the semidiurnal internal tide is expected to travel away. This is representative of the situation in the midlatitude oceans. The model domain is 135 km wide with a depth of 100 m on the shelf and 200 m offshore. For simplicity, the slope between the shelf and the offshore region has a linear profile, with the corners at the shelf break and at the bottom of the slope being rounded over a few grid points. Figure 1 shows the middle portion (-30 to 30 km) of the model, within which the horizontal and vertical resolutions are 300 and 3.3 m, respectively. The regions outside of this portion are sponge zones over which the horizontal grid spacing increases linearly by an order of magnitude. The time step of model integration is about 3 min.

The model is forced by a barotropic tide through specification of sea surface fluctuation at the offshore boundary. A radiation boundary condition is used for all other variables at both offshore and inshore open boundaries. At the sea surface, momentum and buoyancy fluxes are set to zero. At the bottom, a slip boundary condition is used for most of the experiments described here. There is a good reason for neglecting bottom friction for the moment: In both observational data and comprehensive models, it is often difficult to cleanly separate baroclinic motions from barotropic ones because of the presence of bottom friction. A common practice to obtain internal tides is to subtract the vertical average from the total tidal field. This of course cannot remove the vertical shears caused by the bottom drag, which would falsely appear as part of the internal tidal field. To prevent this confusion, we simply set the bottom friction to zero so that barotropic tides do not have any shear and internal tides can be clearly determined. For comparison, we will later show a case where bottom friction is retained.

The model experiments described in the following sections all start with a preexisting density front. Two types of fronts, representing either winter or summer conditions, are shown in Fig. 1. These are quasi-equilibrium states obtained from free model runs of geostrophic adjustment. Note that the density contrast across the winter front is set to be the same as that across either the surface or the bottom branch of the summer front. To ensure stability, a small background stratification (about 0.2% of the vertical density gradient

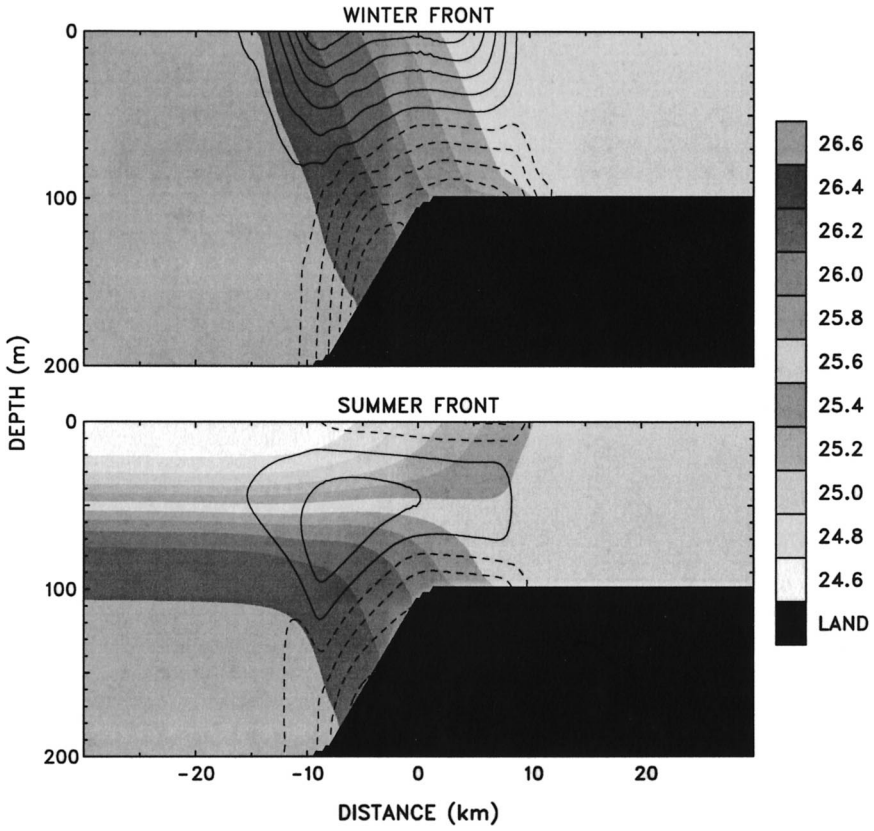

FIG. 1. Initial density (shades) and alongshelf velocity (contour lines) in the middle of the model domain. Contour interval for velocity is 3 cm s^{-1} and dotted lines are for values equal or less than zero (pointing out of paper). Density is in σ_t units.

in the summer pycnocline) is uniformly applied in the model.

3. Winter front

Two sets of experiments are discussed here, one forced with a diurnal (K_1) surface tide and the other with a semidiurnal (M_2) surface tide. The amplitude of the barotropic cross-shelf current is about 16 cm s^{-1} on the shelf in both cases. The model is run for 20 tidal cycles in each experiment and a cyclic quasi-equilibrium state is reached in about 10 cycles. In order to define internal tides and associated density variations, we need to know the barotropic tidal velocity and the tidally advected density field in the absence of the internal tides. These are obtained from two barotropic model runs, which differ from the standard model experiments only in that the internal pressure gradient is set to zero in the momentum equation, so that no internal waves are generated and density is advected as a tracer. The internal tidal field is then simply the difference between the standard and the barotropic model runs with the tidally averaged values subtracted.

Figure 2 shows the density and the cross-shelf flow field during the 20th tidal cycle for the case of diurnal tide. There are four snapshots, 1/4 tidal period apart, for the streamfunctions of both the total tidal flow and the internal tide. The most prominent feature of the internal tide is a large circulation cell confined to the front. It rotates counterclockwise during ebb tide and clockwise during flood tide, causing a surface intensification of the cross-shelf flow. This internal tidal circulation is nearly in phase with the surface tide, being strongest at the maximum ebb and flood and weakest at the slack times. A closer look at the sequence reveals that this single large cell actually evolves from two smaller cells of the same sign, which start to appear around the slack tide. One of them is generated on the lower portion of the seaward side of the front, and the other on the upper portion of the shoreward side of the front. As the tidal flow increases, these cells combine with each other to form a single large cell that extends throughout the front and lasts till the tidal current reverses direction.

This mode of diurnal internal tide is consistent with the analytical model result of Ou and Maas (1988), who predicted that near a winter front the cross-shelf flow would be surface intensified at the diurnal frequency. The physical reason can be explained as follows. During the ebb (flood) tide the front tends to be steepened (flat-

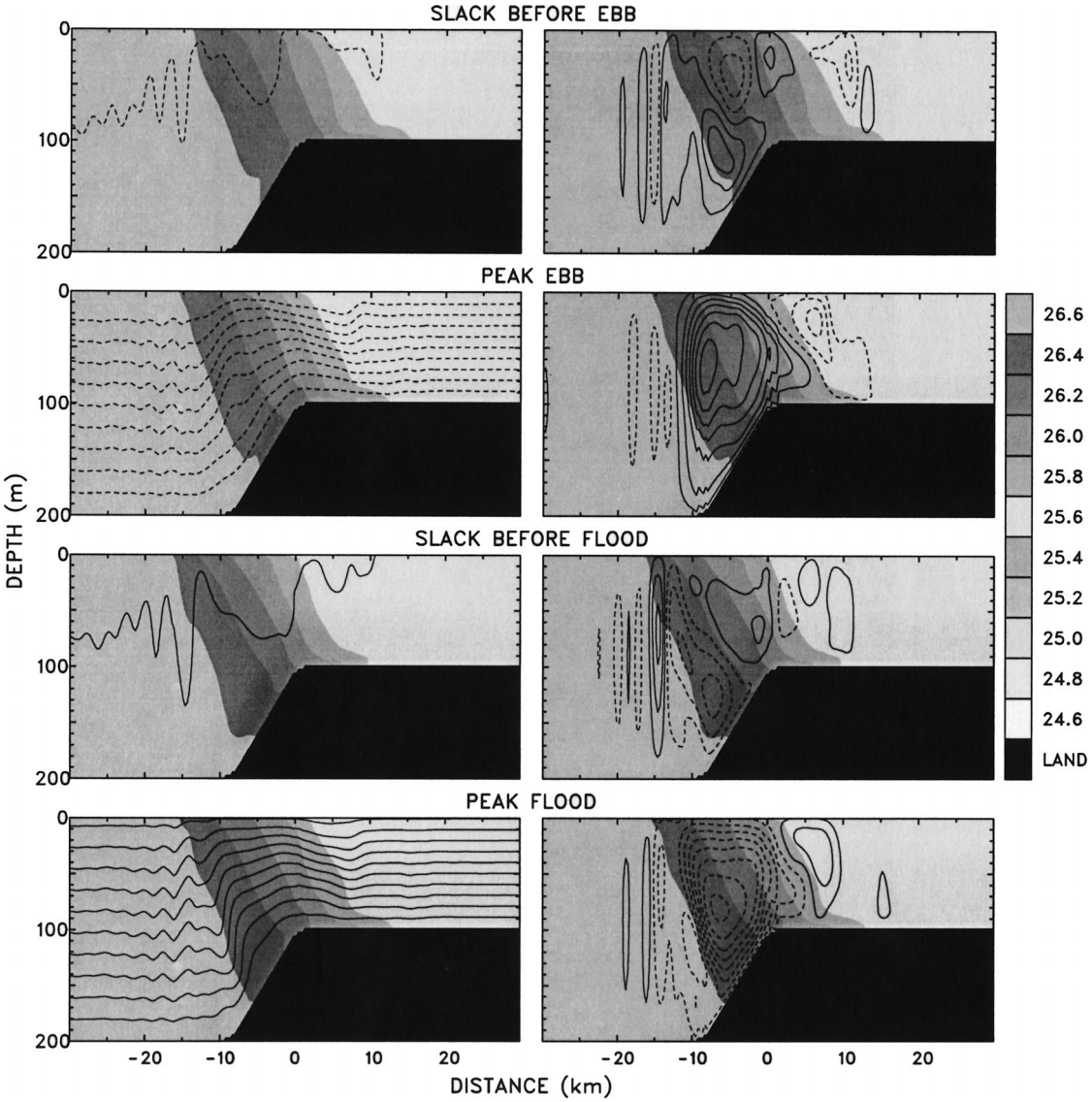

FIG. 2. Cross-shelf streamfunction (contour lines) and density (shades) at four different times, 1/4 tidal period apart, during the 20th tidal cycle for the case of diurnal tide and winter front. Contour interval is 1.5 $m^2 s^{-1}$ for (left) total tidal flow and 0.5 $m^2 s^{-1}$ for (right) internal tide.

tened) by the barotropic tidal current. This is because the barotropic tide that acts on the upper (and farther seaward) part of the front is weaker than that on the lower part of the front due to the sloping bottom topography. To restore the front to its geostrophically balanced position, a circulation cell that rotates counterclockwise (clockwise) tends to be generated in response to the steepening (flattening) of the front. Since the diurnal tidal period is longer than the inertial period here, the geostrophic adjustment is almost instantaneous. Thus the cross-shelf component of the internal tide, which leads the alongshelf component by a quarter of the tidal period, has to be in phase with the forcing that tends to change the front steepness, namely the barotropic tide.

This simple explanation of course cannot count for all the details of the internal tidal field associated with the front. For example, there is a weak cell at the inshore boundary of the front that comes and goes with the large cell within the front but rotates in the opposite direction. It is actually induced by the main internal tidal cell rather than by the barotropic tide since the isopycnals at this boundary are always on the shelf and the barotropic tidal velocity across them is uniform. Along the offshore boundary of the front, there appears to be generation and slow propagation of short internal waves. They escape out of the frontal region and decay within a few wavelengths. Strictly speaking, the wavy features in the weakly stratified offshore water are not internal tides. They are inertial gravity waves excited by the tidal

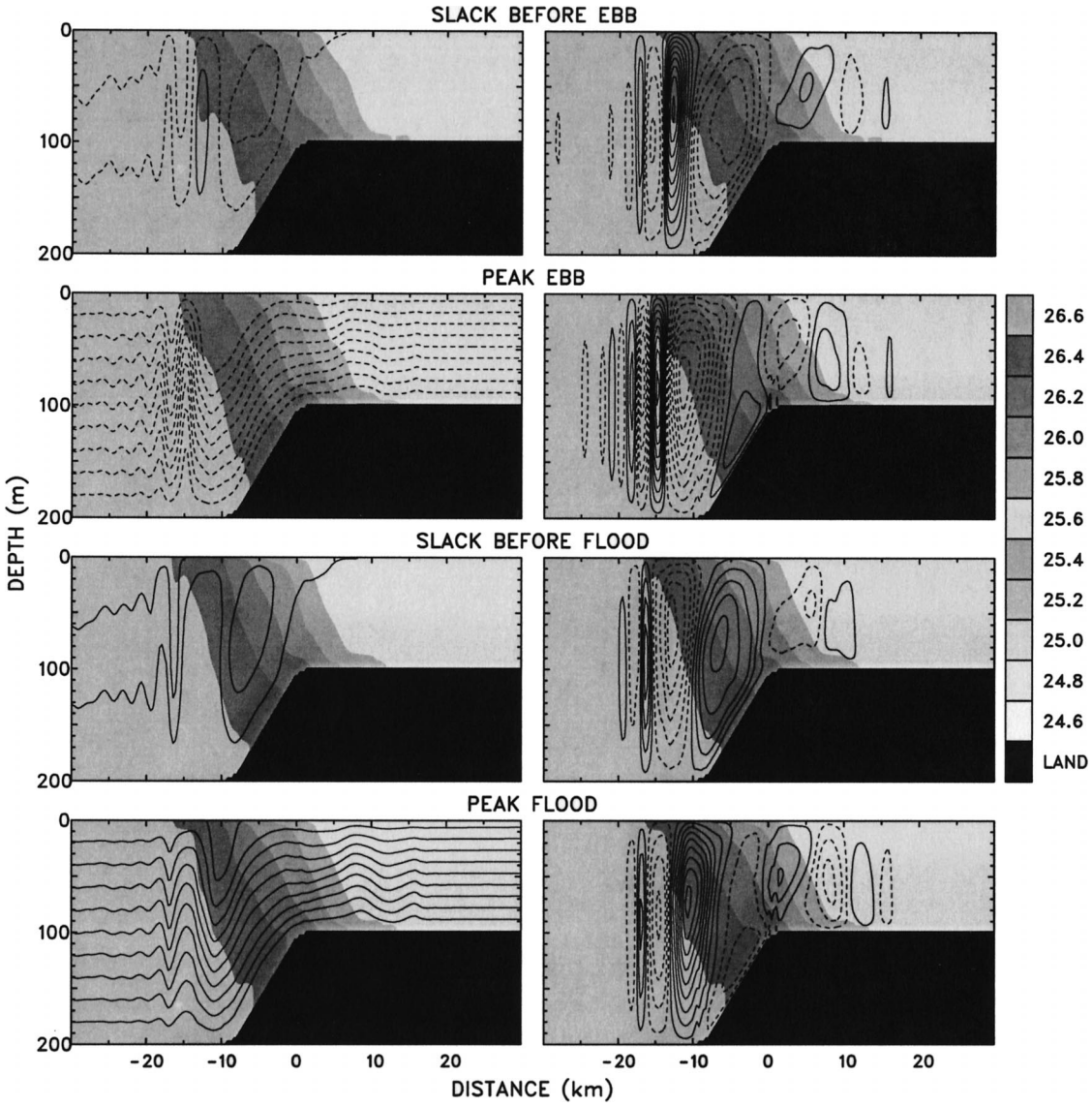

FIG. 3. As in Fig. 2 but for semidiurnal tide.

motions at the frontal boundary. These waves do not carry much energy, but as we will see later, they can cause significant mixing in weakly stratified environment.

The structure of the semidiurnal internal tide at the winter front is quite different from that of the diurnal one. As shown in Fig. 3, the cross-shelf flow is now bottom intensified at the front with a large clockwise internal tidal cell during the ebb tide and a counterclockwise cell during the flood tide. This is again consistent with the prediction of Ou and Maas (1988). The geostrophic adjustment argument that we used above for the diurnal tide can be applied here as well. The difference is that the semidiurnal tidal period is shorter than the inertial period, and thus the internal flow in this case is no longer close to being geostrophic. The time derivative of the internal cross-shelf velocity is proportional to the pressure gradient associated with the front, which lags the barotropic tidal forcing by a quarter of the tidal period. Therefore the internal tidal cell at the front lags the barotropic tide that causes it by half a tidal cycle; the clockwise cell induced by the flood tide actually matures during the ebb tide, and vice versa.

Another big difference between the semidiurnal and diurnal internal tides is that the former apparently propagates away from the site of generation while the latter seems to be dominated by a standing mode. Take the evolution of the counterclockwise cell as an example (see Fig. 3). It starts to appear in the upper slope region at the peak ebb tide. As time proceeds, it grows upward and propagates both seaward and shoreward, with the seaward propagation being more obvious. By the time

of the peak flood, the cell has split into two, a large strong cell going offshore and a small weak cell going onshore. The same sequence takes place for the clockwise cell in the next half tidal cycle. As these internal cells move toward the boundaries of the front, their wavelength and speed continue to decrease due to decreasing stratification, forming a train of tightly packed alternating cells. As they finally move out of the front, they become strongly dissipated and excite a train of inertial gravity waves, which are also eventually lost to dissipation.

The preference of the internal tides to propagate seaward indicates a supercritical bottom slope, while in fact the slope is chosen here to be subcritical according to the classic theory of internal tides (i.e., the bottom slope is less than the slope of the internal wave characteristics, $[(\omega^2 - f^2)/(N^2 - \omega^2)]^{1/2}$, where ω is the wave frequency, f is the Coriolis parameter, and N is the buoyancy frequency). The contradiction is due to the presence of the front. A front that slopes upward in the opposite direction of the bottom topography could substantially decrease the slope of the internal wave characteristics, and such a front could also enhance the generation of internal tides on the sloping bottom (Chuang and Wang 1981). Another noticeable asymmetry is that the counterclockwise internal tidal cells that move seaward are stronger but narrower than the corresponding clockwise ones, especially when approaching the offshore boundary. This is due to the increasing nonlinear effect as the internal tide propagation gradually slows down.

One way to evaluate the impact of the winter front on the generation and propagation of internal tides is to conduct parallel experiments with and without the front. In the latter case, a vertical stratification corresponding to that in the middle of the front is uniformly applied throughout the model. Figure 4 compares the time evolution of the internal cross-shelf velocity at depth 20 m for different cases. Without the front, the semidiurnal internal tide propagates away from the site of generation in both onshore and offshore directions at a phase speed close to that of the first-mode internal wave. The propagation is apparently modulated by the barotropic tidal flow, especially on the shelf where tidal current is stronger and wave speed is slower. The behavior of the diurnal internal tide in the absence of the front is somewhat unexpected from the linear theory. Although disturbances of diurnal frequency are trapped near the shelf break and the slope, there are waves of semidiurnal frequency traveling away. This secondary semidiurnal internal tide is a result of the nonlinear interaction of the diurnal barotropic and baroclinic tides.

The presence of the winter front seems to have three major effects. First, it enhances the generation of internal tides; second, it preferentially channels the propagating internal tidal energy to the offshore direction; and third, it confines most of the internal tide activities to the frontal region. As compared with the case without the front, the amplification of the diurnal internal tide is particularly large, and is characterized by a tidally advected standing mode that occupies the whole width of the front. The semidiurnal internal tide, on the other hand, is strongest at the boundaries of the front due to the energy concentration associated with the refraction of the propagating internal tidal wave. There is no visible reflection at the boundaries because of the strong dissipation there. In both diurnal and semidiurnal cases, there is a small amount of energy leaking out of the front, carried by slowly moving waves. These waves are quickly damped, and the ones that survive the longest have a frequency close to the inertial frequency since such a frequency relates to the longest possible wavelength for inertial gravity waves.

4. Summer front

The model experiments and analyses performed for the winter front are repeated for the summer front. Figures 5, 6, and 7 discussed in this section are the same plots as in Figs. 2, 3, and 4 in the previous section except for a different type of front. The differences and similarities between the internal tides at the summer front and those at the winter front should become obvious by comparing the corresponding pairs of figures.

The structure of the diurnal internal tide at the summer front (Fig. 5) is generally similar to that at the winter front (Fig. 2). The dominant feature is a large internal circulation cell in phase with the barotropic tide, rotating counterclockwise during the ebb tide and clockwise during the flood. The main difference from the winter front case is that the cell here is weaker and less developed in the upper water column so that there is no obvious surface intensification. The upper branch of the front, due to its opposite pressure gradient, limits the growth of the circulation cell induced in the lower branch. The internal tide is still against the barotropic tide near the bottom, but it enhances the barotropic tide more in the middle of the water column than near the surface. According to the reasoning used for the winter front case, such a cell makes perfect sense because it tends to restore both lower and upper branches of the front to their geostrophically balanced position. Another difference between the summer cell and the winter one is that the former is broader and extends farther offshore. This is obviously because the existence of the pycnocline allows more energy to escape out of the front.

The situation is completely different for the semidiurnal tide (Fig. 6). The internal tidal field is now characterized by energetic traveling circulation cells in both offshore and onshore directions. The cells that propagate seaward have much longer wavelength and faster phase speed due to deeper water depth and stronger stratification. The first mode still dominates, but higher vertical modes are evidently present since the cells change their orientation as they travel along. The internal tidal energy actually propagates along the characteristics, going forward as well as up and down. As compared with the

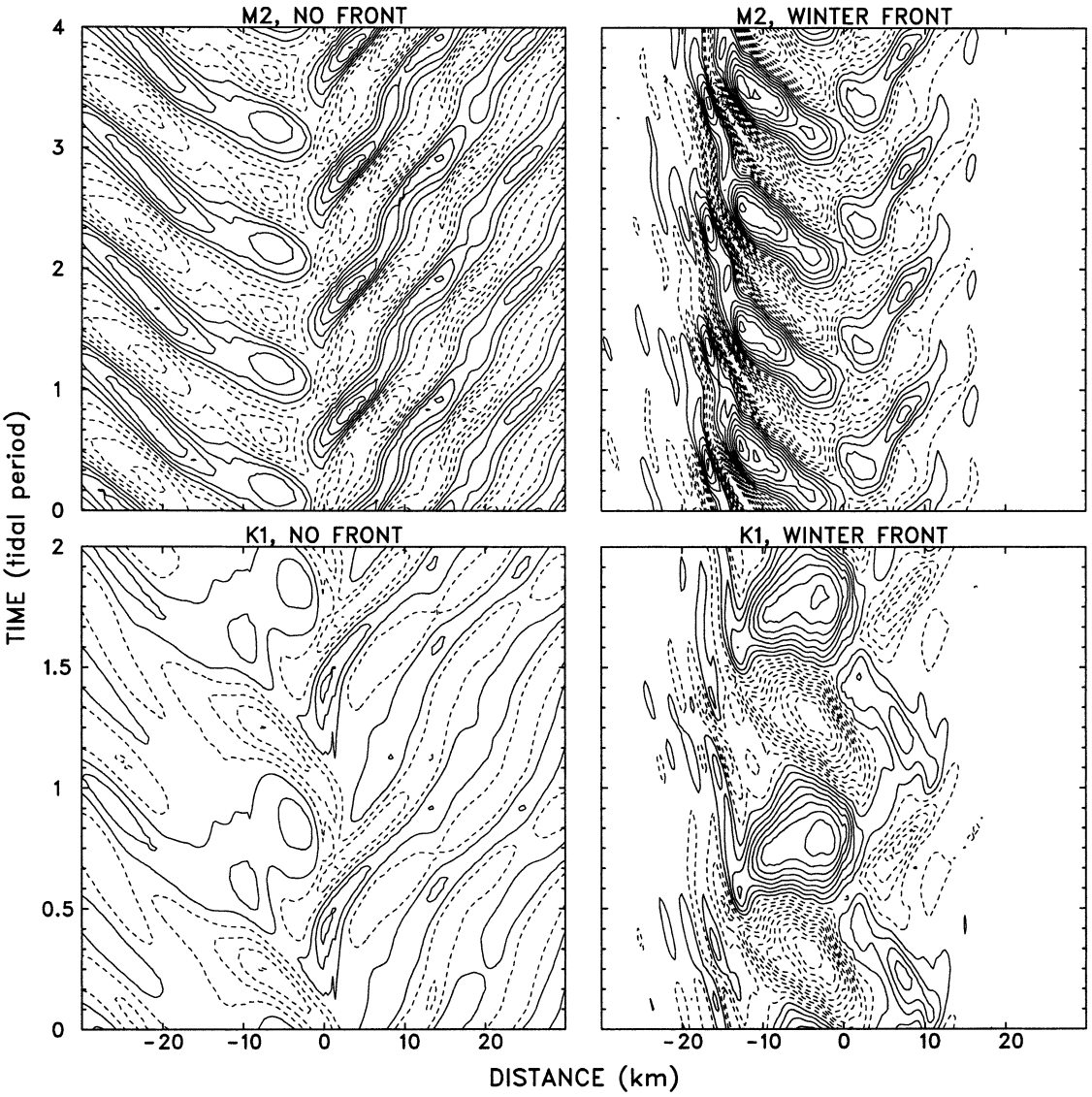

FIG. 4. Time evolution of cross-shelf velocity at depth 20 m for cases (right) with or (left) without front. Contour interval for velocity is 1 cm s^{-1}.

semidiurnal internal tide at the winter front (Fig. 3), there are two major differences here. First, the internal tidal cells are no longer trapped at the offshore boundary of the front because the pycnocline enables them to propagate away. Second, the internal tide no longer preferentially propagates seaward because the upper branch of the front, which slants upward in the direction of the bottom slope, allows a substantial portion of the internal tidal energy to radiate onshore.

Although the same physical process is responsible for the generation of the semidiurnal internal tide here as in the winter front case, there is no apparent bottom intensification of the cross-shelf flow at the front. The reason is that the internal tidal cells move away from the site of generation so fast that, when they mature, they are already out of the frontal region. Let us again follow the evolution of a counterclockwise cell. At the time of the maximum ebb tide two counterclockwise cells are generated, one in each branch of the front. They quickly grow into a single large cell and start to propagate away. By the time of the maximum flood tide, it has long split into two cells traveling in opposite directions. The large seaward going cell has moved way out of the frontal region and the smaller shoreward going cell has moved onto the shelf, leaving the center of the front to the generation of the following clockwise circulation cell. It is interesting to note that the cells that propagate onshore are strongly refracted toward the inshore boundary of the front, very much like what happened to the semidiurnal internal tide at the offshore boundary of the winter front.

The effects of the summer front are again measured

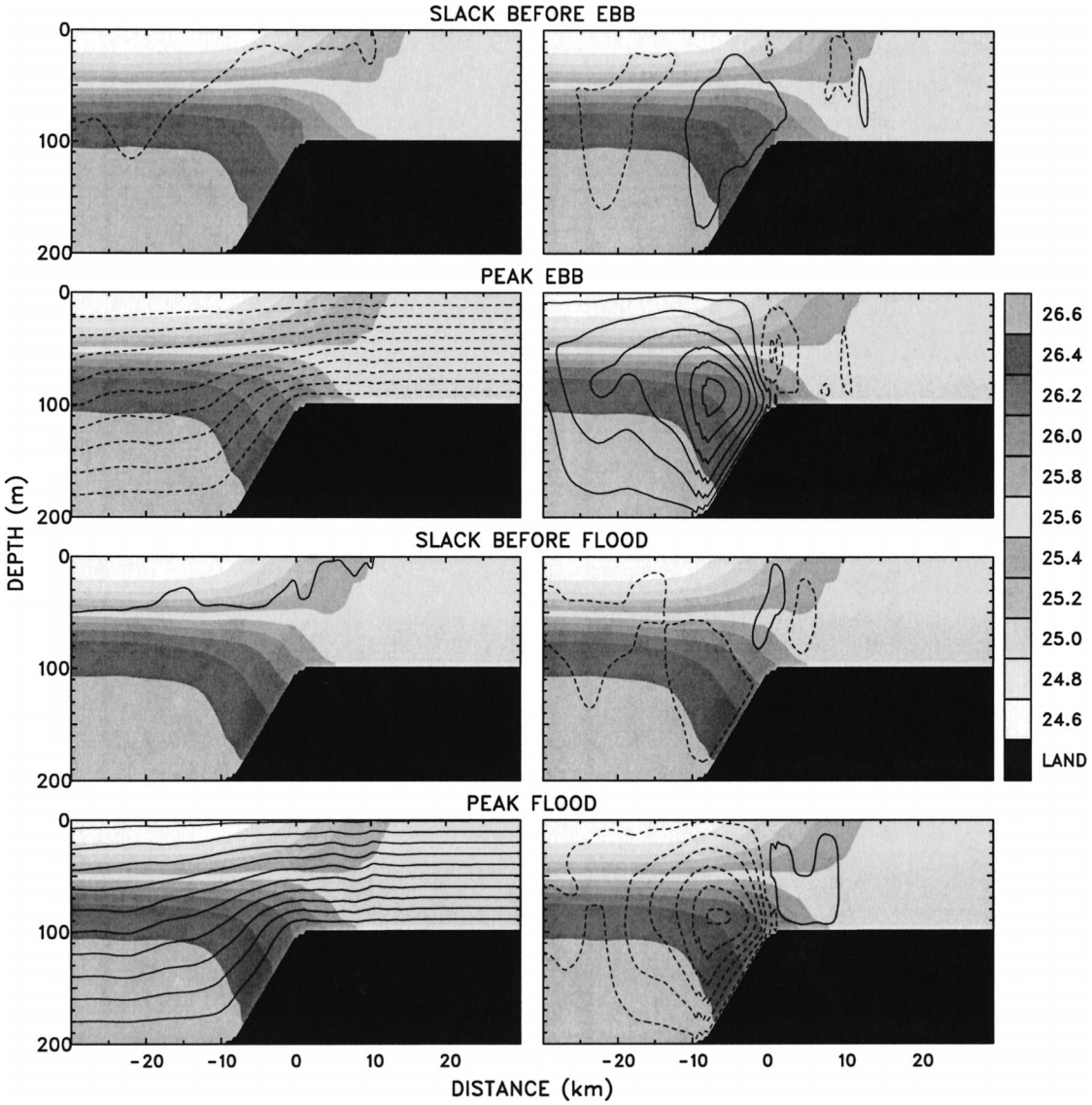

FIG. 5. As in Fig. 2 but for the summer front.

against the case with no front (Fig. 7). The horizontally uniform vertical stratification in the case without the front is chosen to be the same as that of the offshore water in the case with the front. When the front is absent, internal tidal waves propagate away freely from the region of generation in both directions. There is again an indication that part of the diurnal tidal energy is carried away by a nonlinearly produced semidiurnal wave. In the presence of the front, the shoreward propagation is cut short at the inshore boundary of the front. The amplification of internal tides by the summer front is generally not as strong as that by the winter front (see Fig. 4) except at the inshore boundary where the amplitude of the semidiurnal internal tide is largely increased by wave refraction. This, of course, is due to the fact that the summer front has an open end at the offshore pycnocline that allows internal tidal energy to radiate away from the front. Another reason for the remarkable lack of amplification of the diurnal internal tide is that the summer double front does not permit the development of a strong circulation cell that extends from the bottom to the surface, as does the winter single front.

5. Energetics

The kinetic energy of internal tide is simply $\frac{1}{2}[(u - u_T)^2 + (v - v_T - v_G)^2 + (w - w_T)^2]$, where u, v, and w are the cross-shelf, alongshelf, and vertical velocities of the total tidal flow (tidally mean is subtracted), u_T, v_T, and w_T are the corresponding velocities of the barotropic tidal flow, and v_G is the anomalous alongshelf geostrophic velocity associated with the front excursion

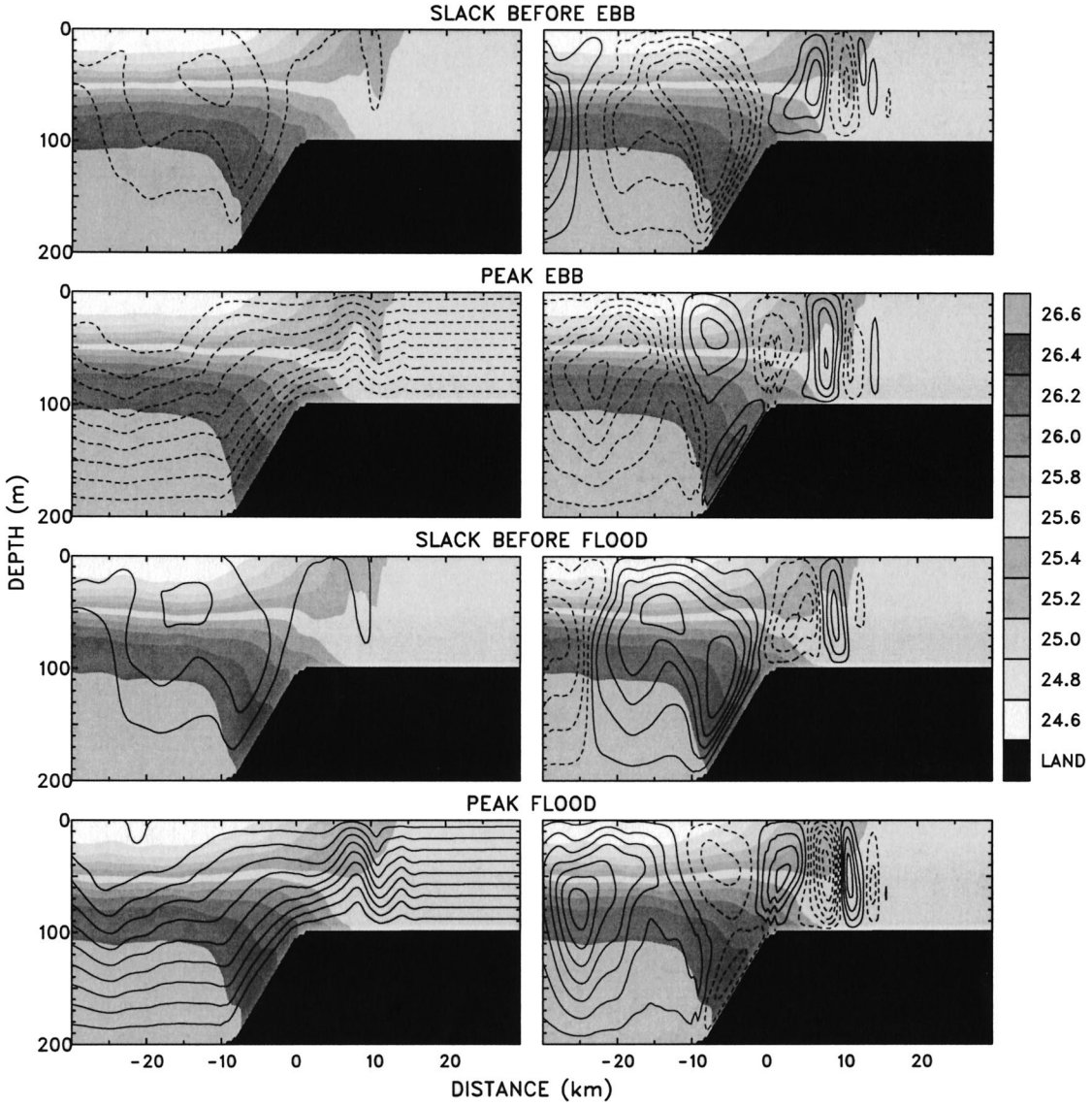

FIG. 6. As in Fig. 3 but for the summer front.

by the barotropic tide. The available potential energy associated with internal tide is estimated as $\frac{1}{2}(g^2\rho'^2/\rho_0 N^2)$ (Gill 1982), where g is gravity, ρ_0 is a reference density, N is the buoyancy frequency of the tidally advected mean density field, and ρ' is the perturbation from the mean. The sum of the kinetic energy and the available potential energy calculated this way defines the total internal tidal energy here.

Figure 8 shows the mean energy density distributions of the internal tides discussed in the previous two sections. In the presence of the winter front, the energy of the diurnal internal tide is mostly confined within the front with maxima near the bottom and the surface, clearly corresponding to the large circulation cell we have seen in Fig. 2. The signature of the smaller cell at the inshore boundary is evident too. The semidiurnal internal tide also has most of its energy trapped to the winter front, but the center of action is now at the offshore boundary rather than the middle of the front. The intense energy density maximum at the offshore corner is apparently due to the strong refraction of the internal tide there. In the case of the summer front, the energy of the diurnal internal tide is still mostly confined in the frontal region though it has a tendency to spread offshore along the pycnocline. The maxima at the bottom and in the separation region of the two frontal branches are associated with the circulation cell seen in Fig. 5.

The only case in which significant internal tidal energy is found outside of the frontal region is the case of the semidiurnal tide with the summer front. The energy radiates away in the offshore direction in a fashion

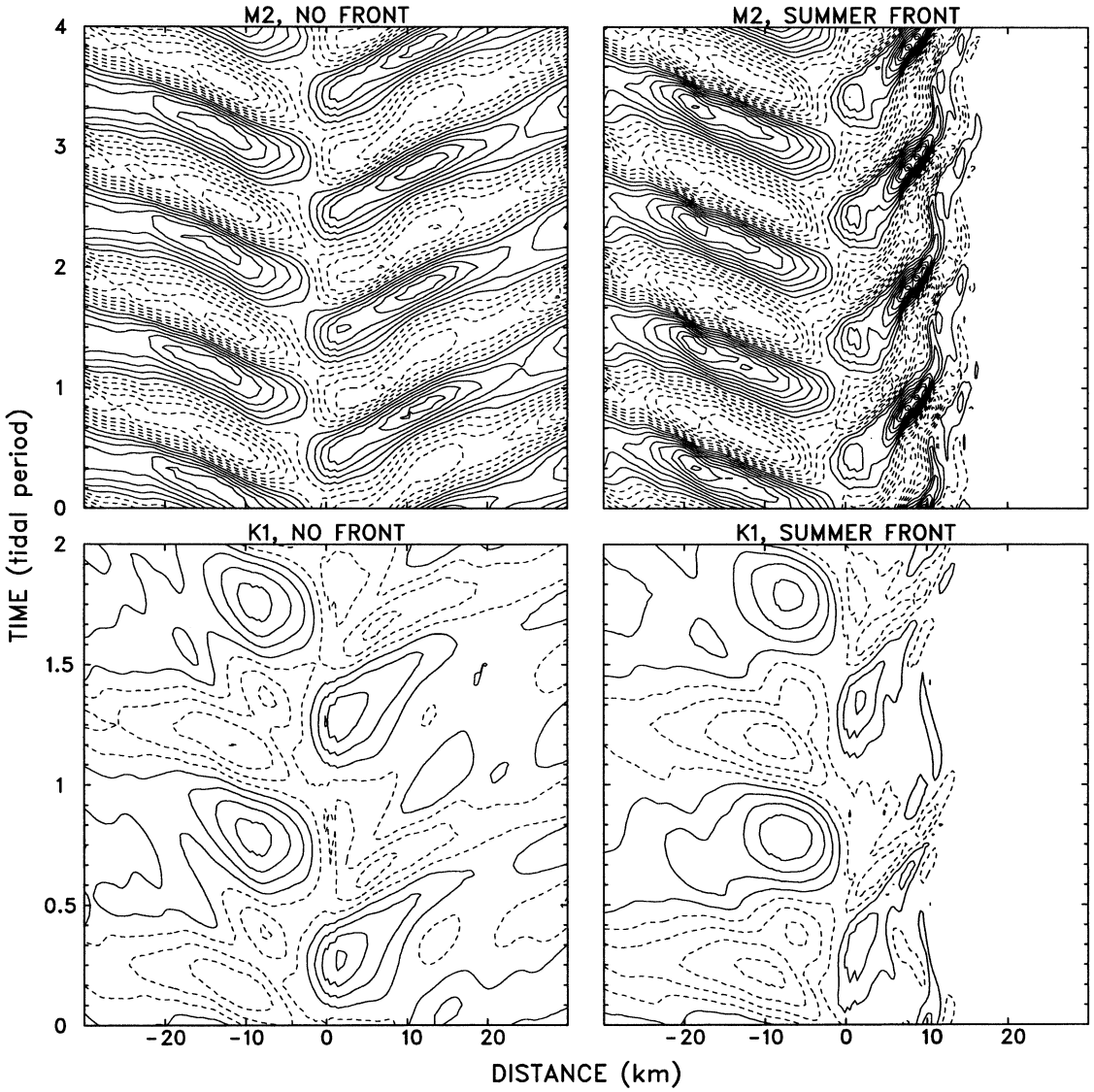

FIG. 7. As in Fig. 4 but for the summer front.

consistent with linear theory, that is, the propagation of the internal tidal energy tends to follow the rays emanating from the shelf break and the slope where the internal tide is generated. Wave refraction and energy concentration occur in places where these rays are reflected from the sea surface. This explains why there are localized maxima in the near-surface velocity, as evident in Fig. 7, for the cases with or without the front. Near the inshore boundary of the front, additional refraction of the internal tide occurs due to diminishing stratification, resulting in particularly strong energy concentration. It is worth noting that in all cases the energy density of the internal tide is relatively high in the bottom layer over the slope, the place where the internal tide is mostly generated, and that the energy there is higher and more closely trapped to the bottom for the diurnal tide than for the semidiurnal tide.

The significance of the internal tide relative to the barotropic tide can be measured by the ratio of their kinetic energies (Fig. 9). The spatial distribution of this ratio is not much different from that of the internal tidal energy shown in Fig. 8, except that the features in the offshore region become more prominent than those on the shelf since the energy density of the barotropic tide decreases as the water depth increases. The kinetic energy of the internal tide is generally much less than that of the barotropic tide, but in some localized places it can be as large as or even larger than the latter. These places include the surface layer in the middle of the winter front for the diurnal tide, the surface layers on the seaward side of the winter front and on the shoreward side of the summer front for the semidiurnal tide, and the energy ray paths of the semidiurnal internal tide in and above the summer pycnocline. It should be point-

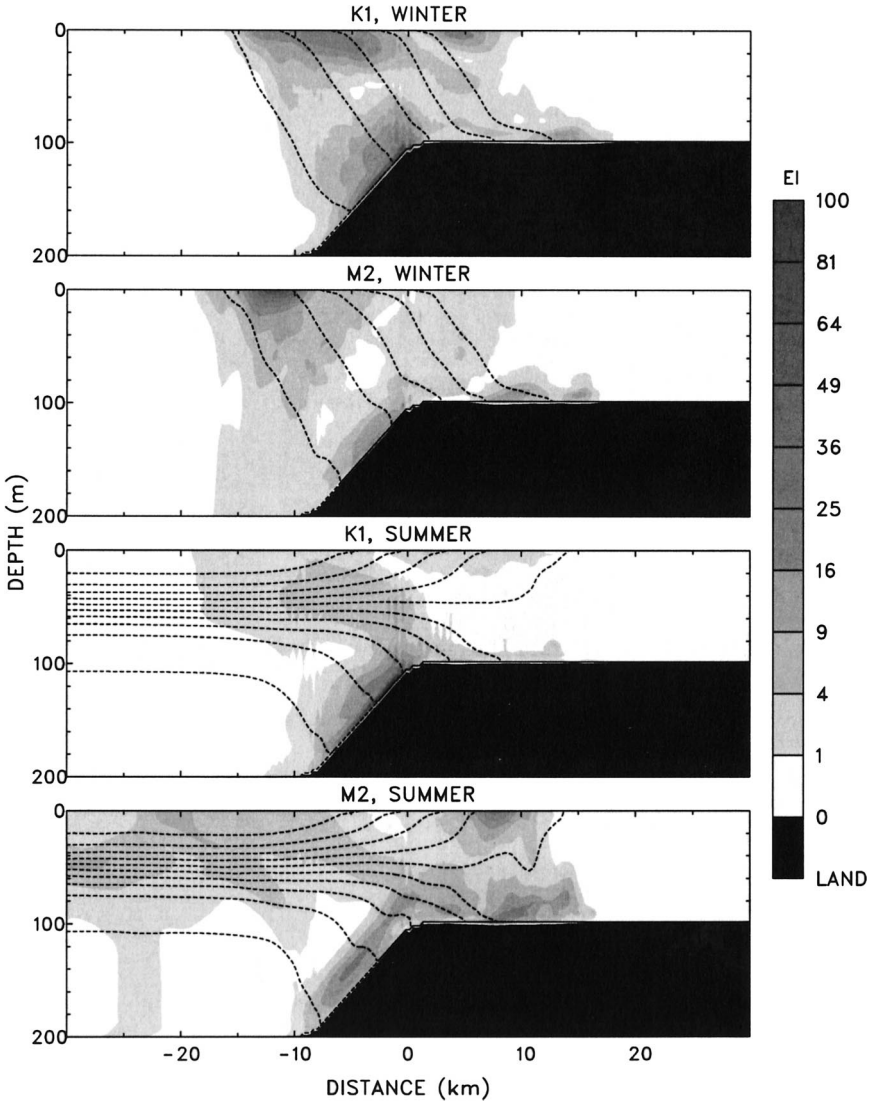

FIG. 8. Mean energy density (J m^{-3}) of internal tides for different cases (shades). Density field is shown as dashed contour lines.

ed out that internal tides may play a more significant role in mixing than barotropic tides, even in places where their energy level is much lower than that of the latter, because they provide the main source of velocity shears away from the bottom frictional layer.

On the other hand, the places with a high level of internal tidal energy do not necessarily coincide with the sites of strong mixing and dissipation because turbulence production depends not only on velocity shear but also on density stratification. Figure 10 shows the spatial distribution of the turbulent kinetic energy (TKE), which is calculated here prognostically using the turbulence closure of Mellor and Yamada (1982). As compared with the distribution of the internal tidal energy (Figs. 8 and 9), the most striking difference is the lack of activity in the summer pycnocline. There the shears of the energetic internal tides are not large enough to overcome the strong stratification. In all cases the TKE is intense in the bottom layer over the slope where internal tides are strong and stratification is weak. For the same reason, large TKE values are found at the offshore boundary of the winter front and the inshore boundary of the summer front for the case of semidiurnal tide. While there is a moderate turbulence production throughout the winter front by either diurnal or semidiurnal internal tide, the relatively strong stratification keeps the TKE level very low in the middle water column of the summer front.

6. Mixing effects

We evaluate the mixing effects of internal tides by including a passive tracer in the model. In order to have an overall picture, the tracer is placed on a grid with a

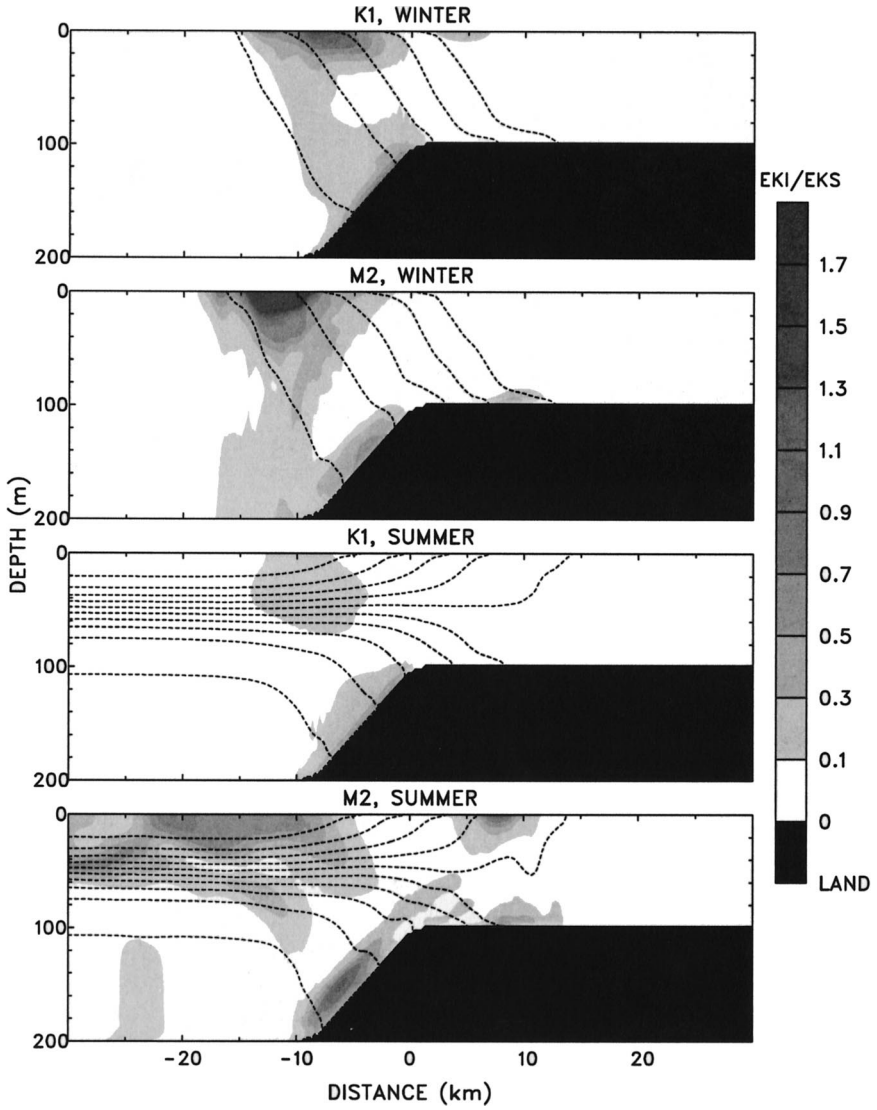

FIG. 9. Ratio of mean kinetic energy of internal tide to that of surface tide for different cases (shades). Density field is shown as dashed contour lines.

horizontal spacing of 6 km and a vertical spacing of approximately 33 m. The horizontal grid lines are 10 m thick and the vertical grid lines are 1.2 km wide. This grid of a tracer is released at the slack before the ebb tide, after the model has reached a cyclic quasi-equilibrium in each one of the model experiments described in the previous sections. The model is then run for several tidal cycles more and the evolution of the tracer field is recorded. To avoid the complication due to tidal advection, we only check the tracer field at successive slacks before the ebb. In such a sequence, the changes in the tracer distribution result mainly from the mixing by internal tides and the advection by tidally averaged residue currents. We do not have a clean way to separate these two here, but the latter should be less important than the former in the first few tidal cycles after the tracer release.

Figure 11 displays the evolution of the tracer field over six tidal cycles in the case of the semidiurnal tide for both winter and summer fronts. Many features in this figure are consistent with what one would expect from the TKE distribution (Fig. 10). The vertical mixing is very strong at the offshore boundary of the winter front and the inshore boundary of the summer front. There is intense mixing in the bottom boundary layer for both fronts, but only for the winter front the mixing takes place in the whole water column throughout the frontal region. The fact that the tracer is mixed horizontally as well as vertically cannot be directly attributed to the TKE distribution since in our model formulation only the vertical mixing term is related to the TKE. The horizontal mixing here is mostly caused by shear dispersion, a process in which vertical mixing acts upon an oscillatory shear flow to spread a tracer hori-

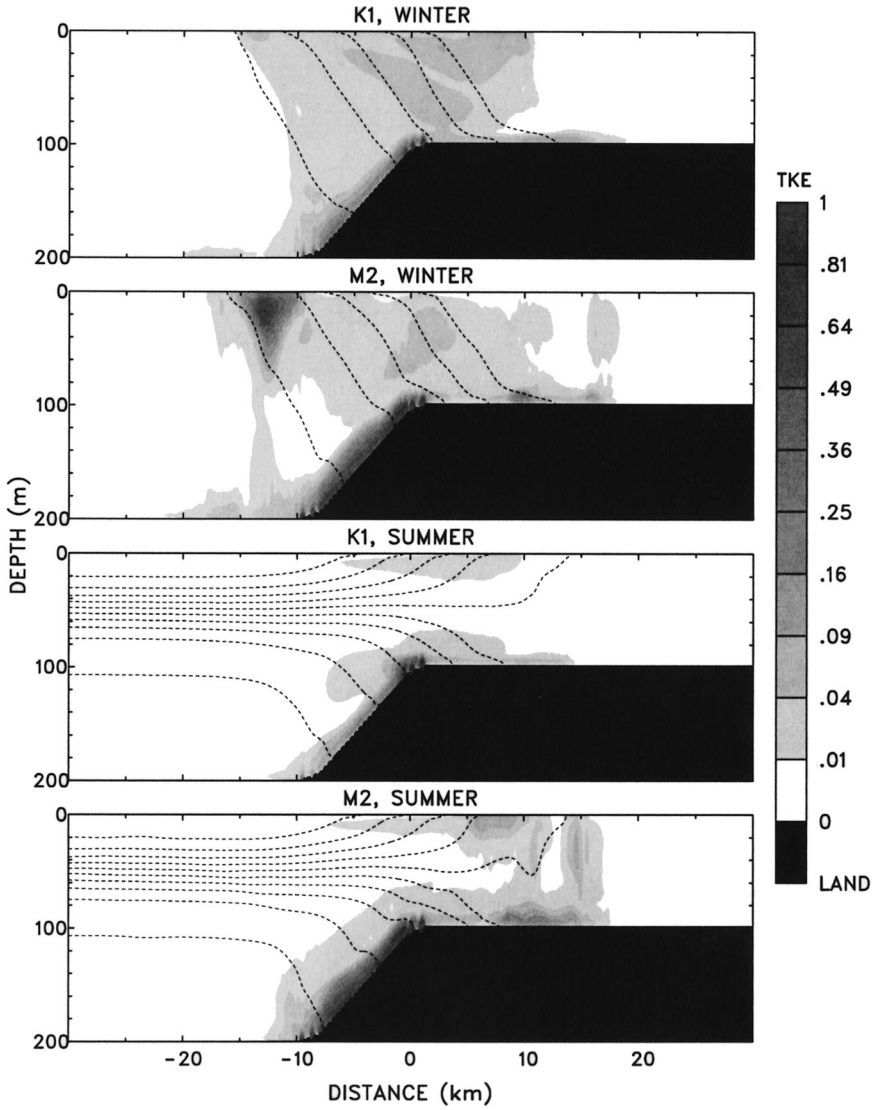

FIG. 10. Mean turbulent kinetic energy (J m^{-3}) for different cases (shades). Density field is shown as dashed contour lines.

zontally. The largest dispersion occurs in the bottom layer over the slope where both the shear and the TKE are intense. The tracer distribution does not change much outside of the frontal region, except for the wiggles associated with the inertial gravity waves seaward of the winter front. Some persistent distortions of the tracer grid are evidently caused by the residue flow.

The corresponding plots for the case of diurnal tide are shown in Fig. 12. As expected, there is little mixing in the summer front except near the bottom, while strong vertical mixing and horizontal dispersion take place throughout the winter front. The main difference from the case of semidiurnal tide is that vertical mixing is not nearly as strong at the offshore boundary of the winter front and the inshore boundary of the summer front, but the mixing in the middle of the winter front is somewhat stronger. It is evident in Figs. 11 and 12 that density is much more resilient to mixing than the tracer. The density field does not change much from one tidal cycle to another while the tracer grid is being rapidly mixed. This seems odd because both density and tracer are acted upon by the same diffusive and advective processes. To understand this, we need to clarify a couple of points. First, density is not a passive tracer; it interacts with the dynamical processes to determine the state of the system. Second, in our experiments the tracer is put into the model when a quasi-equilibrium state has already been attained. In such a state, density changes little because its diffusion is balanced by advection, but a newly introduced tracer field will be strongly altered by the dynamical processes that seem to have no effect on the density, unless its spatial distribution is exactly the same as that of the density.

In all the experiments so far, we used a slip bottom

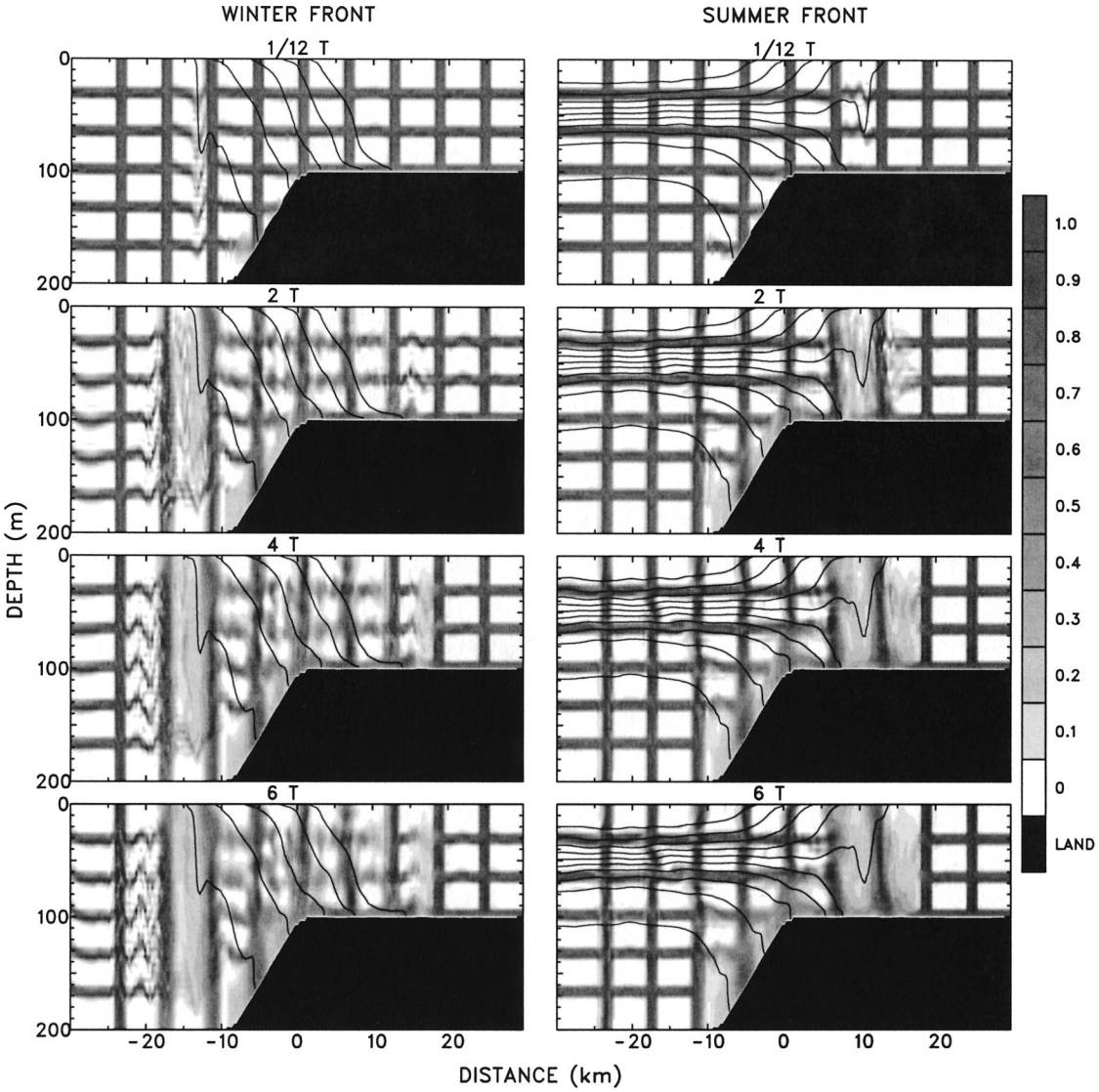

FIG. 11. Tracer distribution at different times after release for the case of semidiurnal tide with either (left) winter or (right) summer front. Density field is shown as dashed contour lines.

boundary condition on purpose to prevent the internal tidal field from being contaminated by the shears of the surface tide due to bottom friction. Now the question is to what extent this simplification is valid or, in other words, how the internal tides obtained this way will be affected by retaining the bottom friction. This is exactly what we show in Fig. 13, which is the same as Fig. 11 except the corresponding experiments include bottom friction. Away from the bottom boundary layer, the results from the cases with bottom friction are almost identical to those without. The main impact on the front by retaining bottom friction is a strong shoreward intrusion at the foot of the front. This is due to an Ekman transport associated with the bottom stress on the alongshelf geostrophic flow. To a much less extent, such a shoreward bottom intrusion also exists in the case without the bottom drag since the vertical shear in the geostrophic current (Fig. 1) can produce an internal stress. The addition of the bottom drag greatly enhances this process. In the weakly stratified regions outside of the front, the effect of the bottom friction is to create a thick bottom mixed layer through largely increased vertical mixing.

It is worth noting that there is little horizontal dispersion in places where internal tides are absent, even when strong vertical mixing is generated there by the bottom-dragged surface tide. For example, on the inner shelf shoreward of both the winter and summer fronts, there is no internal tidal activity (Fig. 11). In the presence of bottom friction, the surface tide produces a 60-m-thick bottom mixed layer there and completely destroys the horizontal tracer grid lines in that layer, but

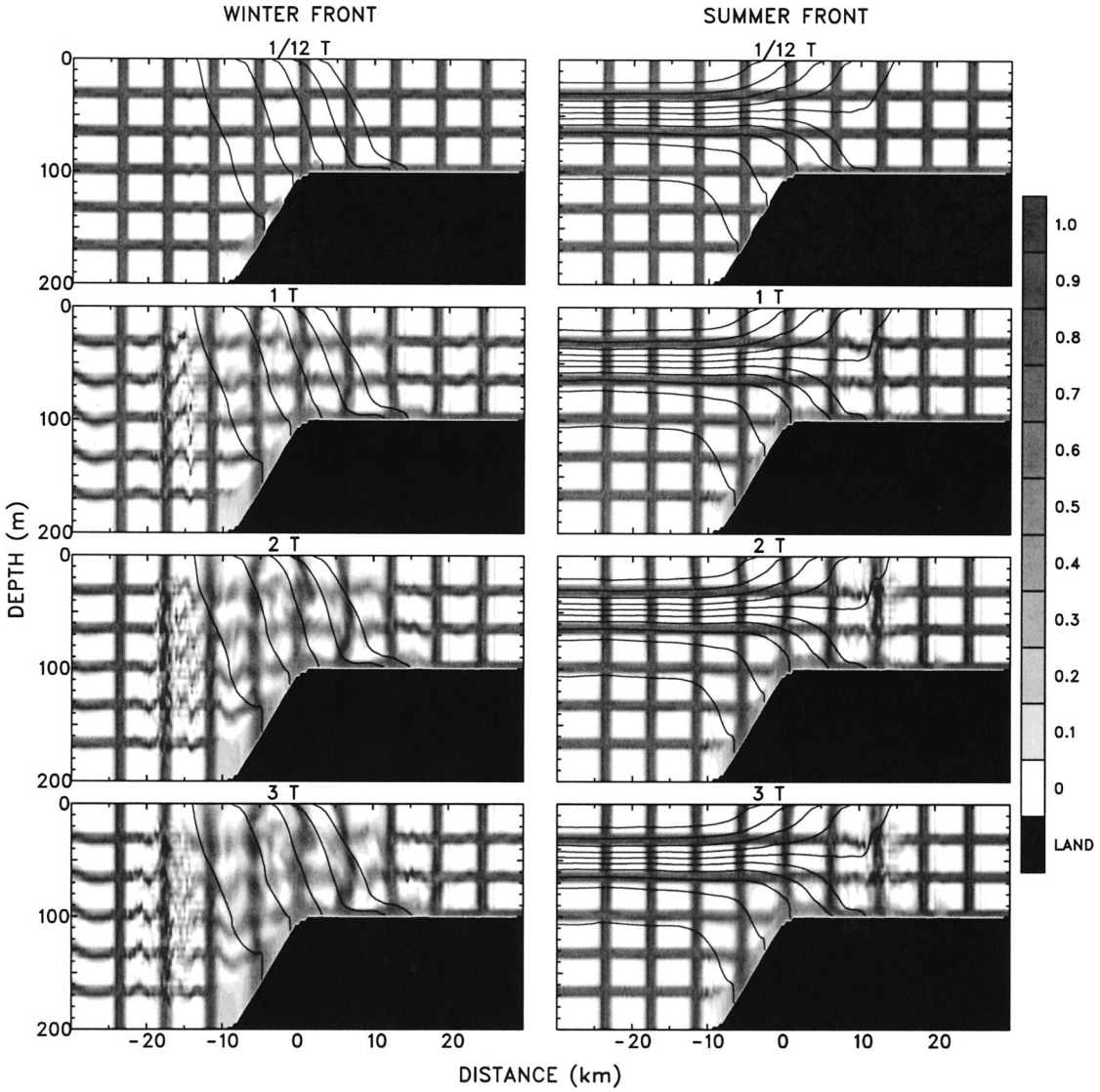

FIG. 12. As in Fig. 11 but for diurnal tide.

it does not have a significant effect on the vertical tracer grid lines (Fig. 13). This implies that, at least for the parameter range used in this study, the shears associated with internal tides are larger than those caused by bottom friction. Horizontal dispersion is not likely to be effective without the internal tides even within the bottom mixed layer. Above this layer, the internal tides certainly play a dominant role in mixing and dispersion, if atmospheric forcing is not considered.

7. Summary and discussion

We have studied the internal tides in the coastal frontal zone near the continental shelf break using an idealized numerical model, with emphases on their structure, energetics and mixing effects. The model is set to represent either winter or summer conditions at a mid-latitude location, and it is forced with a surface tide of either diurnal or semidiurnal frequency. We found that the properties of internal tides are highly dependent on frontal configuration and tidal frequency. At the winter front, energetic internal tides are generated and arrested in the frontal zone; the cross-shelf flow tends to be surface (bottom) intensified by a large internal circulation cell at the diurnal (semidiurnal) frequency. At the summer front, the diurnal internal tide is still trapped, but the semidiurnal internal tide travels out of the frontal zone in the offshore direction while arrested at the inshore boundary. The internal tides can cause significant mixing and dispersion in both winter and summer fronts; the semidiurnal internal tide has the strongest effects toward the frontal boundaries while the diurnal internal tide is more effective close to the site of generation.

The presence of a shelf–slope front enhances the gen-

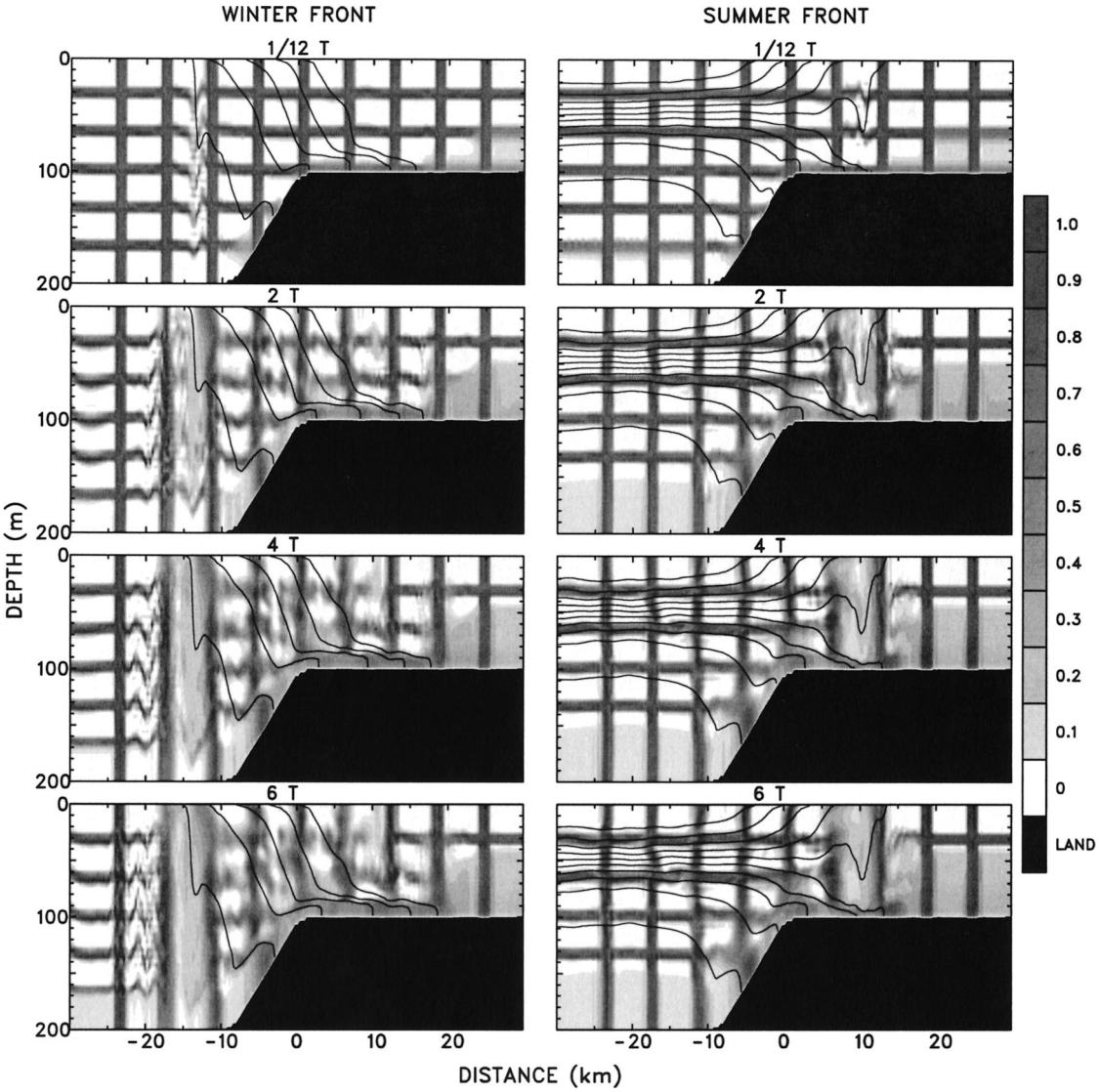

FIG. 13. As in Fig. 11 but for the case with bottom friction.

eration of internal tides, especially during winter time. This is attributable to larger disturbances of the density field by the surface tide because the isopycnals in the front are more perpendicular to the barotropic tidal flow over the slope. The presence of the front also causes a further amplification of the semidiurnal internal tide by trapping its energy in the frontal zone. This amplification is most prominent at the offshore boundary of the winter front and at the inshore boundary of the summer front, where strong refraction of the internal tide takes place. The effect of the summer front on internal tides differs from that of the winter front in at least three ways: first, the existence of the summer pycnocline permits internal tidal energy to quickly radiate away to the open ocean; second, the structure of the summer double front does not allow the development of a large bottom-to-surface internal circulation cell as does the winter front; and third, the upper branch of the summer front facilitates a shoreward propagation of the semidiurnal internal tide, while the winter front preferentially channels it seaward.

The surface (bottom) intensification of the cross-shelf flow of the diurnal (semidiurnal) tide at the winter front is consistent with the theoretical prediction of Ou and Maas (1988). Bottom intensified semidiurnal tide has also been identified in other observational and modeling studies (e.g., Holloway 1984; Chen and Beardsley 1995). However, another prediction of Ou and Maas (1988), the preferential amplification of the semidiurnal tide relative to the diurnal tide is not evident in the present model. Their theory is based on a linear, inviscid model, which allows the existence of standing modes in a front with closed ends. Since the eigenfrequencies of these modes have a lower cutoff at the inertial fre-

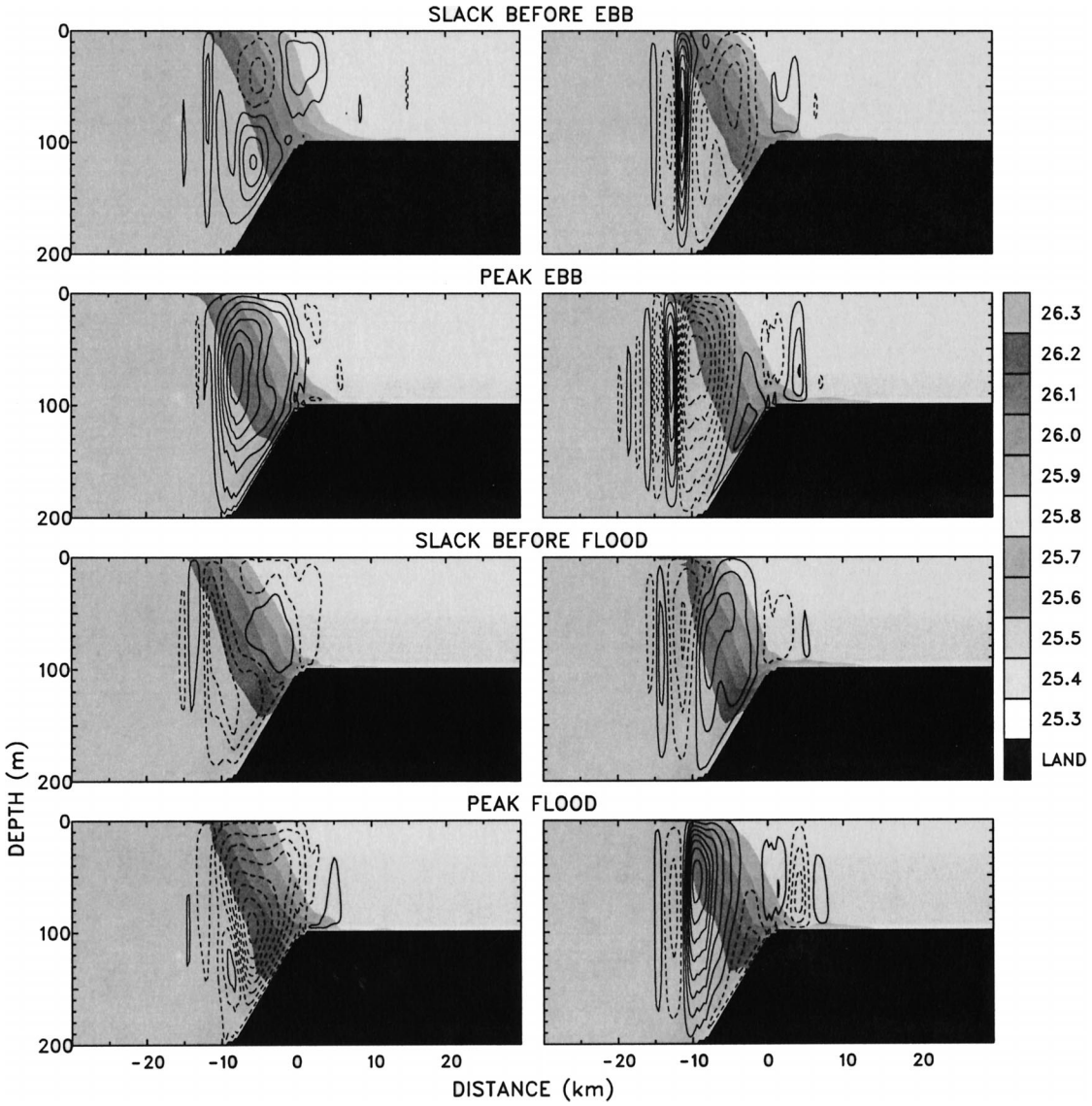

FIG. 14. (left) Diurnal and (right) semidiurnal internal tidal fields similar to those shown in Figs. 2 and 3 except for a winter front that is only half as wide as the original one.

quency, the semidiurnal tide is preferred for resonance with one of the superinertial modes. It seems that in the present model there are no standing modes for the progressive semidiurnal internal tide. This is because of the lack of reflection from the ends of the front where the refracted semidiurnal tide is dissipated almost completely. Therefore, the energetic semidiurnal tide found in this model, which has maximum energy density toward the frontal boundaries, is a result of refraction rather than resonance.

Our model results are not particularly sensitive to the choice of physical parameters such as the width of the front and the slope of the bottom topography. For example, Fig. 14 shows the internal tidal fields at a winter front that is 50% narrower than the original one. The similarity between these fields and those shown in Figs. 2 and 3 is quite remarkable. All of the description and discussion presented in section 2 is still valid here, though the propagation of the semidiurnal internal tide is limited to a narrower frontal zone. We also did an experiment with the front widened by 50% (not shown). The diurnal internal tidal cell again remains trapped to the slope, while the semidiurnal tide propagates farther offshore and onshore to the frontal boundaries. The effect of bottom slope on internal tide generation is well known from theory, and what we found in our sensitivity study is consistent with the theory. In short, a critical slope is most favorable for internal tide generation; a supercritical slope prevents internal tides from propagating onshore; and a subcritical slope is less effective in generating internal tides. As mentioned earlier, the bottom slope in the model is subcritical when only ver-

tical stratification is considered, but for the winter front it becomes slightly supercritical. Increasing or decreasing the slope by 50% only changes the magnitude and the onshore/offshore partition of internal tides, but not their general structure and behavior.

The model experiments discussed here are generally in a weakly nonlinear regime. The tidal flow is subcritical except when internal tides are highly refracted near the frontal boundaries, in which case nonlinearity becomes important. This results in an asymmetry in the semidiurnal internal tide, as evident in Figs. 3 and 4. What is not shown here is that the nonlinearity also generates a residue flow field that is dominated by a series of alternating circulation cells with the spatial scales of the internal tides. This kind of rectification has also been found in previous theoretical and modeling studies (e.g., Maas and Zimmerman 1989; Chen and Beardsley 1995). Another instance in our experiments that points to the importance of nonlinearity is the occurrence of a near-semidiurnal wave in the case of diurnal forcing (Fig. 4). The implication is that, when the nonlinear interaction between surface and internal tides becomes more important, a significant portion of the diurnal tidal energy will no longer be trapped to the site of generation, and any observed semidiurnal tidal field may partly result from diurnal surface tide. We will explore in a subsequent paper the interaction between internal tides and coastal fronts in a strongly nonlinear regime.

Acknowledgments. This research is supported by the National Science Foundation through Grant ATM 9618260. We thank two anonymous reviewers for their helpful comments.

REFERENCES

Baines, P. G., 1982: On internal tide generation models. *Deep-Sea Res.,* **29,** 307–338.

Brickman, D., and J. W. Loder, 1993: Energetics of internal tide on northern Georges Bank. *J. Phys. Oceanogr.,* **23,** 409–424.

Chen, C., and R. C. Beardsley, 1995: A numerical study of stratified tidal rectification over finite-amplitude banks. Part I: Symmetric banks. *J. Phys. Oceanogr.,* **25,** 2090–2110.

——, and ——, 1998: Tidal mixing and cross-frontal particle exchange over a finite amplitude asymmetric bank: A model study with application to Georges Banks. *J. Mar. Res.,* **56,** 1163–1201.

Chen, D., and D.-P. Wang, 1990: Simulating the time-variable coastal upwelling during CODE 2. *J. Mar. Res.,* **48,** 335–358.

Chuang, W.-S., and D.-P. Wang, 1981: Effects of density front on the generation and propagation of internal tides. *J. Phys. Oceanogr.,* **11,** 1357–1374.

Gill, A. E., 1982: *Atmosphere–Ocean Dynamics.* Academic Press, 662 pp.

Holloway, P. E., 1984: On the semidiurnal internal tide at a shelfbreak region on the Australian North West Shelf. *J. Phys. Oceanogr.,* **14,** 1787–1799.

——, 1996: A numerical model of internal tides with application to the Australian North West Shelf. *J. Phys. Oceanogr.,* **26,** 21–37.

Huthnance, J. M., 1989: Internal tides and waves near the continental shelf edge. *Geophys. Astrophys. Fluid Dyn.,* **48,** 81–106.

Lamb, K. G., 1994: Numerical experiments of internal wave generation by strong tidal flow across a finite amplitude bank edge. *J. Geophys. Res.,* **99,** 843–864.

Maas, L. R. M., and J. T. F. Zimmerman, 1989: Tide–topography interaction in a stratified shelf sea, II: Bottom trapped internal tides and baroclinic residual currents. *Geophys. Astrophys. Fluid Dyn.,* **45,** 37–69.

Mellor, G. L., and T. Yamada, 1982: Development of a turbulence closure model for geophysical fluid problems. *Rev. Geophys. Space Phys.,* **20,** 85–875.

Ou, H. W., and L. R. M. Mass, 1988: Tides near a shelf–slope front. *Cont. Shelf Res.,* **8,** 729–736.

Smagorinsky, J., 1963: General circulation experiments with the primitive equations. I: The basic experiment. *Mon. Wea. Rev.,* **91,** 99–164.

Smolarkiewicz, P. K., 1984: A fully multidimensional positive definite advection transport algorithm with small implicit diffusion. *J. Comput. Phys.,* **54,** 325–36.

Wang, D.-P., 1982: Development of a three-dimensional limited-area (island) shelf circulation model. *J. Phys. Oceanogr.,* **12,** 605–617.

——, 1985: Numerical study of gravity currents in a channel. *J. Phys. Oceanogr.,* **15,** 299–305.

——, D. Chen, and T. J. Sherwin, 1990: Coupling between mixing and advection in shallow sea fronts. *Cont. Shelf Res.,* **10,** 123–136.

Wunsch, C., 1975: Internal tides in the ocean. *Rev. Geophys. Space Phys.,* **13,** 167–182.